Audio Engineering Society

Convention Paper

Presented at the 142nd Convention
2017 May 20–23, Berlin, Germany

This paper was peer-reviewed as a complete manuscript for presentation at this convention. This paper is available in the AES E-Library (http://www.aes.org/e-lib) all rights reserved. Reproduction of this paper, or any portion thereof, is not permitted without direct permission from the Journal of the Audio Engineering Society.

Interactive Display of Microphone Polarity Patterns with non-fixed Frequency Point

Jonathan D. Ziegler[1,2], Hendrik Paukert[1], and Bernfried Runow[1,2]

[1] *Stuttgart Media University, Institute for Electronic Media, Nobelstr. 10, 70569 Stuttgart, Germany*
[2] *University of Tübingen, Visual Computing, Sand 14, 72076 Tübingen, Germany*

Correspondence should be addressed to Jonathan D. Ziegler (zieglerj@hdm-stuttgart.de)

ABSTRACT

With the development of bidirectional and unidirectional microphones dating back to the 1930's, the parameter of directivity has been an integral aspect of microphone construction for nearly 100 years [1]. This characteristic is commonly visualized with the microphone's sensitivity displayed as a radius *r* over a 360 - degree span within a polar coordinate system. Measured directivity is generally shown as an overlay of well-defined frequencies [2]. Although this is common practice, in-depth analysis of the actual performance of a microphone is difficult. In this paper, a novel approach to displaying the directional characteristics of a microphone is presented, providing an interactive display of the angular sensitivity at any frequency. Furthermore, the application within microphone array development is discussed.

1 Introduction

The directional sensitivity of a microphone is traditionally displayed as a theoretical plot within a polar coordinate system (polar plot). As shown in Figure 1, more information can be extracted from measurement data, which is generally given at a few select frequencies defined by IEC60268 [3]. This method provides minimal insight into the actual frequency-dependent angular sensitivity of the microphone. Moreover, using a more prominent line type for lower frequencies or showing plots of non-IEC60269 frequencies may cause misperceptions. Frequencies below 2 kHz generally show near optimal angular sensitivity. This paper proposes a method for providing frequency-dependent directivity information. A prototype application is introduced and data interpolation and smoothing for different applications are presented.

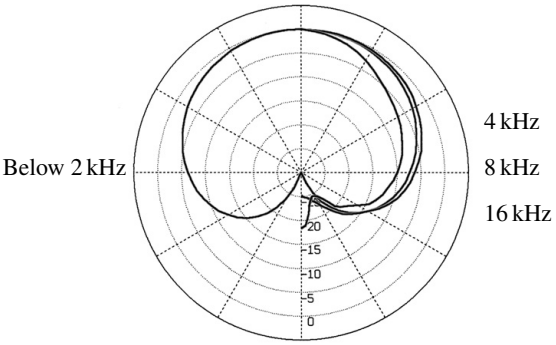

Fig. 1: Traditional display of directive microphone sensitivity at frequencies defined by IEC60268 [2]. The overlapping plots make exact observations about the frequency-dependent angular sensitivity difficult.

2 Methods

2.1 Data Acquisition

To acquire all necessary information to describe the angle- and frequency-dependent microphone sensitivity $S(\theta, \nu)$ impulse responses (IR's) were gathered:
In an anechoic chamber meeting ISO 3745 Precision Class 1 standards [4], sine sweep test tones of 3 s were played back using a high quality studio monitor at approximately 4 m distance from the microphone. The test tone was recorded at $n = 24$ rotation positions of the microphone, set via a motorized rotation device connected to the microphone stand and monitored with the appropriate software. The resulting recordings, representing an angular resolution of 15°, were deconvolved with the sweep signal to aquire the impulse responses. These were later treated to reduce the influence of loudspeaker imperfections by deconvolving the signals with an impulse response of the speaker, recorded with a high quality measurement microphone prior to the IR-recordings. The microphone's power spectrum at the angle $(n-1)\cdot 15°$ can be accessed via Discrete Fourier Transform (DFT) [5].

The resulting power spectra can be seen in Figure 2. The observed irregularities at higher frequencies are largely due to the fact that multiple microphone capsules were combined in a shock-mount during recording of the impulse responses. This causes reflections, leading to interference effects which can drastically increase or decrease sound pressure at arbitrary locations and frequencies.

2.2 Frequency Smoothing

Many applications require a certain degree of data smoothing. For the power spectra shown in Figure 2, $\frac{1}{N}$ - octave smoothing with $N = 12$ was applied. Some marketing brochures show data smoothed with up to $N = 3$. Figure 3 shows an IEC61260-compliant $\frac{1}{N}$ - filter bank with $N = 3$ [6].

2.3 Angle Interpolation

To get from 24 steps, represented by $S_i(\nu)$, to full 360° resolution as shown in Figure 4, described with $S(\theta, \nu)$, cubic spline data interpolation is applied. Cubic spline interpolation is achieved by constructing third-order polynomials within every interval $[S_i(\nu)\,,\, S_{i+1}(\nu)]$ with $i = 0, \ldots, n-2$.

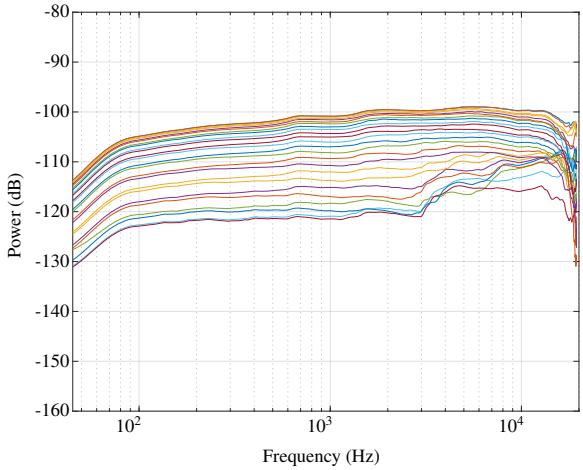

Fig. 2: Power spectra of measured microphone capsule in 15°- steps around a full rotation. Data smoothing with $\frac{1}{12}$ - octave filterbank is applied.

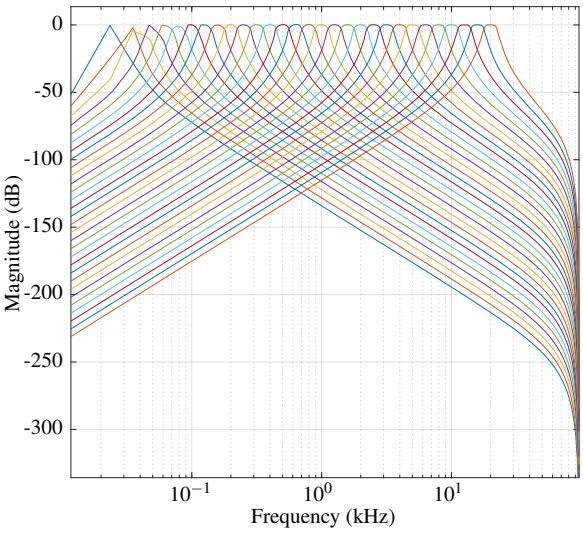

Fig. 3: Magnitude response of IEC61260 - compliant $\frac{1}{3}$- octave filter bank used to smooth frequency responses [6]. The filters shown result in strong smoothing, whereas more accurate data can be retained by applying filter banks with narrower bands.

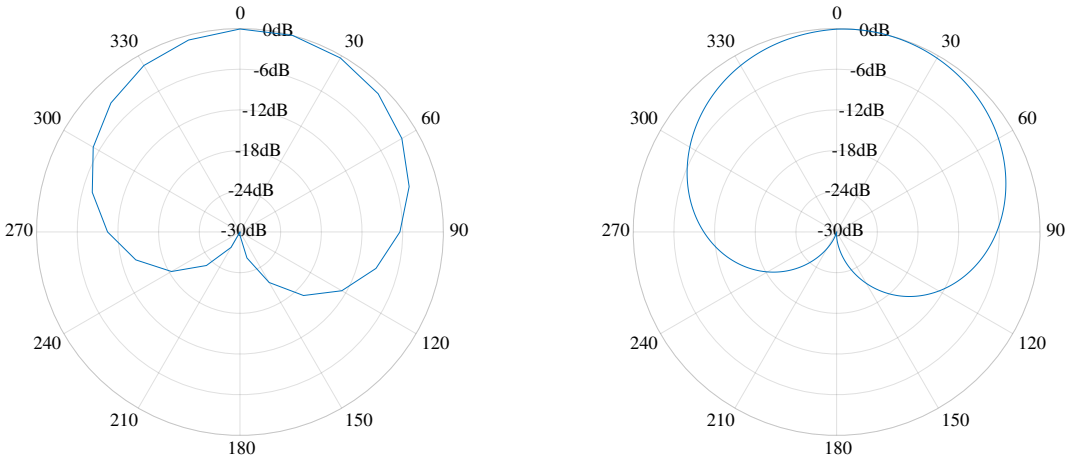

(a) Before interpolation. The 24 data points for the given frequency bin are simply connected with lines.

(b) After interpolation the polar graph shows great resemblance to the theoretical curve for cardioid directivity.

Fig. 4: Interpolation process of angular sensitivity plot. Figure 4a shows the contours of a polarity plot with measured data simply connected by lines. This creates a rough and improbable graph. Figure 4b shows a version which has been interpolated with an angular resolution of 1° using cubic splines.

Considering the i^{th} part of the spline Y_i we get ([7, 8]):

$$Y_i(\tau) = a_i + b_i\,\tau + c_i\,\tau^2 + d_i\,\tau^3 \tag{1}$$

where τ is a parameter between 0 and 1. This results in

$$Y_i(0) = S_i = a_i \tag{2}$$
$$Y_i(1) = S_{i+1} = a_i + b_i + c_i + d_i \tag{3}$$

The derivatives of Y_i with respect to τ at the points S_i then are

$$Y'_i(0) = b_i \tag{4}$$
$$Y'_i(1) = b_i + 2c_i + 3d_i \tag{5}$$

Required boundary conditions are matching splines in all measurement points, as well as matching first- and second-order derivatives. Therefore we get

$$Y_{i-1}(1) = S_i \tag{6}$$
$$Y_i(0) = S_i \tag{7}$$
$$Y'_{i-1}(1) = Y'_i(0) \tag{8}$$
$$Y''_{i-1}(1) = Y''_i(0) \tag{9}$$

Additionally, to guarantee a sufficient number of boundary conditions to be able to solve the $4(n-1)$ unknowns, the second derivative of the endpoints is set to zero.

$$Y''_0(0) = 0 \tag{10}$$
$$Y''_{n-2}(1) = 0 \tag{11}$$

The conditions for a correct interpolation of the directivity patterns discussed in this paper are the demand for 360°- 0° continuity and a continuous derivative in the mentioned interval. As cubic spline interpolation guarantees both conditions (see equations 2, 3, and 8), simple data wrapping between 360° and 0° suffices for these conditions to be met. Therefore we set

$$S_{24} := S_0 \tag{12}$$

and solve for all 4n variables a_i, b_i, c_i and d_i at all frequencies ν.

With certain directivities, such as hypercardioid and figure-of-eight, transitions into areas of negative sensitivity have to be addressed. Figure 5a shows an example, where the transition between positive and negative sensitivity was not taken into account in the interpolation process. Figure 5b shows the corrected version.

3 Results

The resulting application prototype is capable of converting a dataset of $m \times n$ impulse responses of m microphones, recorded at n angles, sampled at up to 192 kHz, into an interactive polar plot. Current research has focussed on capsules with cardioid and figure-of-eight directivity characteristics, although any arbitrary directivity is possible. As the processing relies on simple

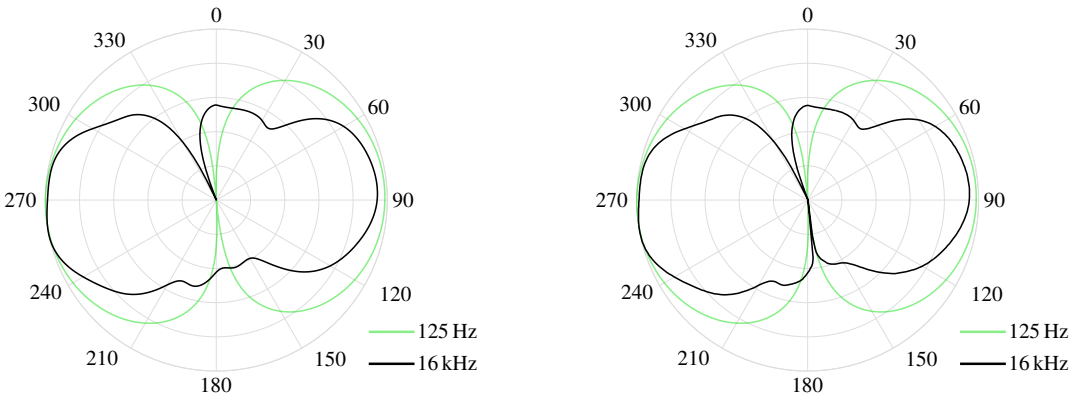

(a) No correction at $\pm$ - transition.

(b) Correct interpolation.

Fig. 5: Interpolation errors occurring in the transition area between positive and negative sensitivities. Not taking this into account can lead to distorted directivity plots, especially at high frequencies, where the measured angular sensitivity shows more deviation from the theoretical curve.

impulse responses, the software is not restricted to single-capsule setups. Monophonic coincident arrays of any type can be evaluated as well (see Figure 6). Smoothing and normalization guarantee a seamless experience when sweeping through the frequencies. Figure 6 shows a screenshot of the prototype, displaying the measurements of a Schoeps double-M/S setup at approximately 1 kHz. The angle of the array towards the loudspeaker during IR-capturing was slightly off-axis, resulting in an offset of θ. As the setup was mounted in a common shock-mount, the same offset applies to all three capsules. For the potential use as a marketing instrument, offset correction can be applied.

4 Discussion

Through the use of interactive frequency-dependent angular sensitivity displays, the performance of a given microphone can be assessed in greater detail than with traditional polar plots. This can be advantageous when used as marketing material for high-performing microphones, or to help engineers find weaknesses in current hardware design. A promising aspect of the presented application is the evaluation of the performance of beamforming arrays. Figure 7 shows the polar response of a synthesized supercardioid, created with the double-M/S configuration shown in Figure 6,

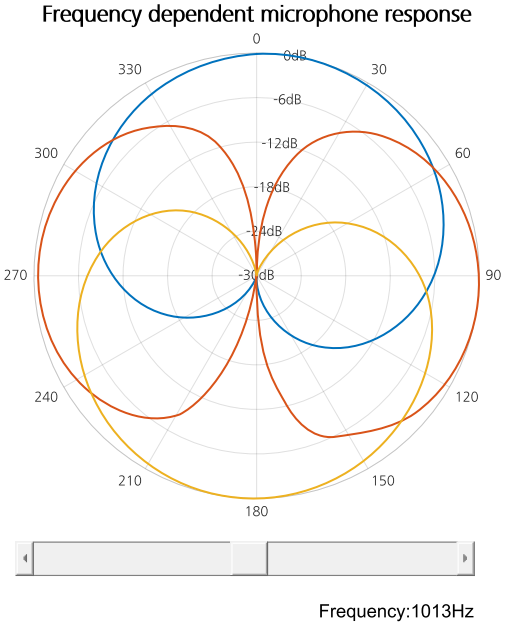

Fig. 6: Application prototype displaying measurements of a Schoeps double-M/S setup consisting of two CCM 4 cardioid capsules and one CCM 8 figure-of-eight capsule at $\approx$ 1 kHz [2].

using the synthesis models shown in equations 13 to 16 [10]. The use of this application for continuous performance monitoring of beamforming algorithms can be a useful aid for DSP development and quality assessment.

Using the microphone configuration shown in Figure 6, an arbitrary 1^{st} order directivity pattern can be synthesized, oriented towards any desired angle.

The signal from pressure sensors $p(\theta,t)$ and pressure gradient sensors $g(\theta,t)$ can be combined using:

$$S(\theta,t) = \alpha\, p(\theta,t) + (1-\alpha)\, g(\theta,t) \tag{13}$$

For this example, using a double-M/S setup, the pressure sensor (omnidirectional signal) is synthesized using the front- and rear-facing cardioids:

$$p(\theta,t) = S_{frontC}(\theta,t) + S_{rearC}(\theta,t) \tag{14}$$

For the desired supercardioid we set ([9]):

$$\alpha = \sqrt{2} - 1 \tag{15}$$

Using equations 13 - 15 we can compute a supercardioid as shown in Figure 7, using:

$$\begin{aligned} S_{SC}(\theta,t) = (\sqrt{2}-1)\left(S_{frontC}(\theta,t) + S_{rearC}(\theta,t)\right) \\ + (2-\sqrt{2}) S_{fig8}(\theta,t) \end{aligned} \tag{16}$$

Although current parameters show promising results and good performance, further research is required to determine optimal frequency-smoothing for different applications. Also, interpolation using n^{th} degree spherical harmonics instead of cubic splines could lead to better results for areas with changing sensitivity polarity as found in figure-of-eight directivity patterns, and for areas with a large angular derivative of the signal $\left(\left|\frac{\mathrm{d}S(\theta,v)}{\mathrm{d}(\theta)}\right| \gg 0\right)$. As the IR recording took place with three microphones simultaneously, an obvious amount of interference can be observed. The rear-facing cardioid microphone shows dramatic distortion of directivity characteristics at frequencies as low as 5 kHz, while the front-facing cardioid capsule of the same model shows relative frequency invariance up to 14 kHz. For more valid results additional IR recordings are needed without the reflective surfaces of elaborate shock-mounts and other capsules.

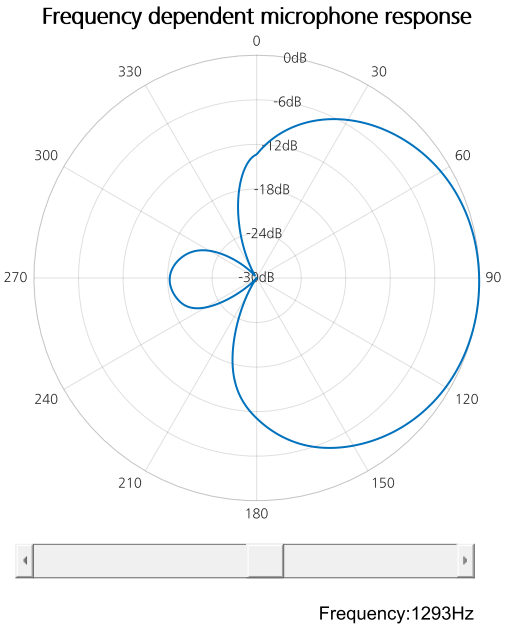

Fig. 7: A synthesized supercardioid response created using signals from the Schoeps double-M/S configuration shown in Figure 6.

5 Summary

A method to capture and interactively display the frequency-dependent angular sensitivity of microphones is introduced. Data capturing via the recording of impulse responses in an anechoic environment is described. Subsequently, signal processing in the form of deconvolution, smoothing, and interpolation are discussed and examples are shown in Figures 4 and 5. A functioning application prototype is introduced and application examples are provided:

- Display of single capsules to assess the quality of frequency invariance of a given directivity pattern (Figure 5b).
- Display of multi-capsule setups to examine the effect of inter-capsule-reflections and microphone mounting (Figure 6).
- Display of synthesized directive signals to assess the quality of beamforming algorithms (Figure 7).

Furthermore, future improvements in data acquisition and processing are discussed.

References

[1] Olson, H. F., "A History of High Quality Studio Microphones," in *Audio Engineering Society Convention 55*, 1976.

[2] *Schoeps Product Catalogue*, Schalltechnik Dr.-Ing. SCHOEPS GmbH, 6 edition, 2016.

[3] *Sound system equipment - Part 4: Microphones*, IEC 60268-4, 2014.

[4] ISO3745, *Acoustics – Determination of sound power levels and sound energy levels of noise sources using sound pressure – Precision methods for anechoic rooms and hemi-anechoic rooms*, 2012, revision 3.

[5] Stein, J. Y., *Digital Signal Processing: A Computer Science Perspective*, Wiley-Interscience, 2000, ISBN 0471295469.

[6] IEC61260, *Electroacoustics - Octave-band and fractional-octave-band filters - Part 1: Specifications*, 2012, revision 3.

[7] Bartels, R. H., Beatty, J. C., and Barsky, B. A., *An Introduction to Splines for Use in Computer Graphics and Geometric Modeling (The Morgan Kaufmann Series in Computer Graphics)*, Morgan Kaufmann Pub, 1987, ISBN 0934613273.

[8] Weisstein, E. W., "Cubic Spline." *MathWorld–A Wolfram Web Resource*, 2017.

[9] Benesty, J. and Jingdong, C., *Study and Design of Differential Microphone Arrays (Springer Topics in Signal Processing)*, Springer, 2012, ISBN 364233752X.

[10] Runow, B. and Curdt, O., "Microphone Arrays for professional audio production," in *28th Tonmeistertagung*, VdT, 2014.